ARTICLE

Application of 2-D and 3-D Geo-electrical Resistivity Tomography and Geotechnical Soil Evaluation for Engineering Site Investigation: A Case Study of Okerenkoko Primary School, Warri-Southwest, Delta State, Nigeria

U. Stanley Eze[1]*, M. Edirin Okiotor[2], J. E. Ighodalo[3], B. Jennifer Owonaro[2], A. Saleh Saleh[4], A. Sikiru Jamiu[2]

[1] *Department of Earth Sciences, Federal University of Petroleum Resources, Effurun, 330102, Nigeria*

[2] *Department of Marine Geology, Nigeria Maritime University, Okerenkoko, Warri South, Delta State, 332105, Nigeria*

[3] *Department of Physics (Applied Geophysics program), University of Benin, Benin City, Edo State, 300213, Nigeria*

[4] *Department of Petroleum Engineering and Geosciences, Petroleum Training Institute, Effurun, 330102, Nigeria*

ABSTRACT

In the design of building structures, joint efforts must be decided to resolve the depth of competent layers across the intended site to safeguard the durability of civil engineering structures and to avert the disastrous consequences of structural failure and collapse. In this study, an integrated methodology that employed DC resistivity tomography involving 2-D and 3-D techniques and geotechnical-soil analysis was used to evaluate subsoil conditions for engineering site investigation at Okerenkoko primary school, in the Warri-southwest area of Delta State, to adduce the phenomena responsible for the visible cracks/structural failure observed in the buildings. The results obtained brought to light the geological structure beneath the subsurface, which consists of four geoelectric layers identified as topsoil, dry/lithified upper sandy layer, wet sand (water-saturated) and peat/clay/sandy clayey soil (highly water-saturated). The deeply-seated peat/clay materials ($\rho \leq 20$ Ωm) were delineated in the study area to the depths of 17.1 m and 19.8 m from 2-D and 3-D tomography respectively. 3-D images presented as horizontal depth slices revealed the dominance of very low resistivity materials i.e. peat/clay/sandy clay within the fourth, fifth and sixth layers at depths ranging from 8.68-12.5 m, 12.5-16.9 m and 16.9-21.9 m respectively. The dominance of mechanically unstable peat/clay/sandy clay layers beneath the subsurface, which are highly mobile in response to volumetric changes, is responsible for the noticeable cracks/failure detected on structures within the study site. These observations were validated by a geotechnical test of soil samples in the study area. Atterberg's limits of the samples revealed plasticity indices of zero. Thus, the soil samples within the depth analyzed were representatives of sandy soil that does not possess any plasticity. The methods justifiably provided relevant information on the subsurface geology beneath the study site and should be appropriated as major tools for engineering site assessment/geotechnical projects.

Keywords: 2D and 3D resistivity tomography; Engineering site/structure; Atterberg limits; Orthogonal lines; Radar sounding

*CORRESPONDING AUTHOR:

U. Stanley Eze, Department of Earth Sciences, Federal University of Petroleum Resources, Effurun, 330102, Nigeria; Email: uchechukwueze2014@gmail.com

1. Introduction

An ample evaluation of geologic and geotechnical subsurface conditions in an intended engineering site is critical for the secure design of building structures, to avert the disastrous consequences of structural failure and collapse prevalent of late. In subsoil evaluation, joint efforts must be decided to resolve the depth to competent layers across the intended site, to safeguard the durability of civil engineering structures i.e. buildings, bridges, roads and other infrastructures [1,2]. On the 1st of November 2021, it was reported that a 21-storey building on Gerard Road, Ikoyi, Lagos State collapsed killing many people, due to lack of quality assurance/control, poor management of the project and negligence by agencies responsible for approval and supervision of the building project [3]. Premium Times report [3], also stated that the building's density and impediment on the site displayed gross negligence of the Lagos State building moderations.

Over 50 percent of all building/structural failures in developing countries like Nigeria can be allied to geologic and geotechnical problems, in accordance with the information provided by Chendo and Obi [4]. The geologic and geotechnical problems cover a wide spectrum from foundation defects caused by poor investigation of the nature/type of soils in the area to the subsurface geology. Areas such as coastal environments, swamp belts and flood plains might have experienced differential sedimentation of diverse organic matters and sediments. These domains are inherently overflowing due to the existence of impermeable soil layer-mostly clay, resulting in the habitation of mechanically unstable peat material (moderately decomposed organic substance) may be imminent [5] as cited in Ayolabi et al. [6].

In evaluating subsoil conditions in an engineering site, the electrical resistivity method, plays a decisive role in the detection of subsoil properties for engineering site probing. Two-dimensional (2-D) geoelectrical resistivity tomography (ERT) is a familiar geophysical imaging technique extensively utilized in environmental and civil engineering investigations [6,7]. The 2-D ERT technique fits the image of both lateral and vertical contrast in ground resistivity measured using electrodes implanted on the surface of the earth [8]. The 2-D resistivity model from a 2-D ERT dataset affords an improved approximation of the subsurface model of the earth [9].

Nevertheless, images resulting from 2-D electrical resistivity surveys often produce misleading subsurface features, due to out-of-plane variation in apparent resistivity anomaly in magnitude and location [10] as cited in Eze et al. [9]. These inaccuracies frequently arise because the basic presumption of two dimensions for geological features is only an approximation. In reality, geological features/structures known in environmental/near surface research are intrinsically three-dimensional (3-D) in the attribute. Therefore, these spurious effects oftentimes lead to errors in the interpretation of 2-D ERT data.

In environmental investigations, where the subsurface geology is frequently complex, subtle and multi-scaled, the objections with 2-D ERT in precisely gauging geometrically complex structures notably in a deeply heterogeneous geologic environment without misconception necessitated the demand for 3-D resistivity imaging which is a more accurate model of the subsurface as reported in the literature [11-15].

In three-dimensional (3-D) resistivity imaging the apparent resistivity magnitudes are recognized to fluctuate in all three directions (vertical, lateral and perpendicular). Therefore, 3-D geoelectrical resistivity imaging with a 3-D model of interpretation should in theory accord a superior interpretation as noted by Loke [16].

Another extensive expression of 3-D resistivity tomography is the capability to array a 3-D resistivity model of the subsurface. A 3-D apparent resistivity volume can be realized and shown in horizontal-depth slices and vertical cross-sectional cuts next to volume rendering. Cross-sectional cuts have the improvement that values of the apparent resistivity in each cell are displayed in all directions (*x-y*, *y-z* and *x-z* planes). From the preceding, the dominance of 3-D ERT to 2-D ERT in detailing complex heterogeneous geological environments cannot be overemphasized, and has been validated in the reports [6,9,13].
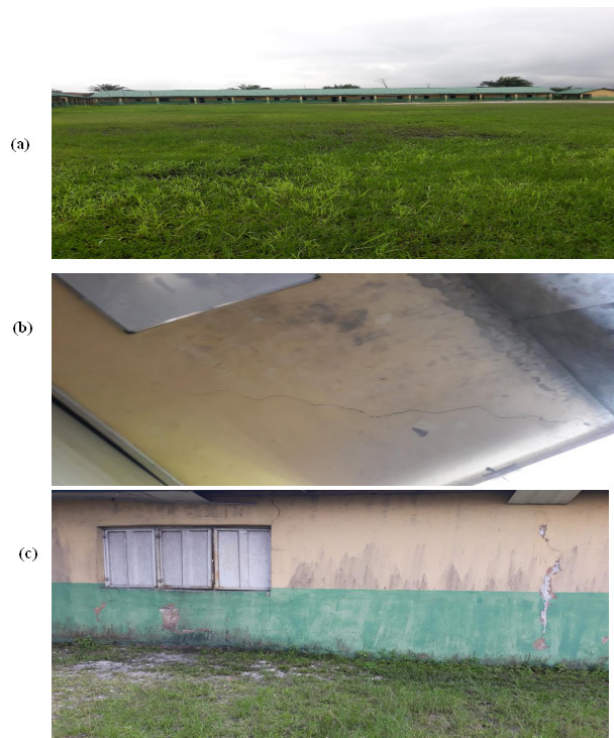
The study area 'Okerenkoko primary school' located in Okerenkoko community in Gbaramatu Kingdom, Warri-south local government area of Delta State, was reported to be suffering from poor maintenance and negligence over a long period of time which has resulted in visible cracks observed in the classroom walls, failure/subsidence and dilapidated buildings (**Figure 1a-1c**). The degree of damage observed in the school building ranges from moderate to severe risk category according to Boscarding and Cording's [17] building damage classification. If nothing is done in addressing the situation, these are warning signs of instability/structural failure that will result in differential settlement of the dilapidated/failed buildings which causes geoenvironmental hazards. It was this extremity that necessitated the adoption of an integrated methodology that employed DC resistivity tomography involving 2-D, 3-D techniques and 1-D VES soundings supported with geotechnical-soil analysis to evaluate the geologic and geotechnical conditions of the subsurface soil and to adduce the phenomena responsible for the structural failure's observed in the school buildings.

In this paper, an orthogonal set of ten (10) 2-D resistivity imaging data all-inclusive of five (5) parallel and five (5) perpendicular traverses were obtained within the school premises (**Figure 1**). The survey was guided, with the objective of assessing the appropriateness of the site for building construction and defining the subsurface geology characteristics beneath the area.

2. Geological setting of the study area and hydrogeology

Okerenkoko community is based in the Gbaramatu Kingdom in the Warri-south local government area of Delta State (Ijaw-ethnic group). The community is positioned between latitude 05°37'39.22" to 05°37'10.12" N and longitude 005°23'30.64" to 005°23'08.79" E. It is stationed within the coastal creeks between the Benin River and the Escravos River (**Figure 2**) that links Warri and Escravos. Vegetation is defined by mangrove forests and rainforests. The Mangrove swamps are low, generally less than about 5 m above sea level.

Figure 1(a-c). Physical condition of the study site (Okerenkoko primary school in Okerenkoko community) as at the time of this study showing the survey location, cracks and dilapidated buildings.

The permanent campus of Nigeria Maritime University is based in this community. Warri Southwest local government is home to the Delta State's Itekiri and Ijaw ethnic groups.

The geology of the Warri-South Okerenkoko region is located in the Niger Delta, and the geology of the region has been examined by many scholars such as Asseez [19]; Reyment [20]; Short and Stauble [21]. The stratigraphic layers of the Niger Delta include the Akata, Agbada and Benin Formations. Typical sections of these formations are briefed in other reports such as Short and Stauble [21]; Doust and Omatsola [22]; Kulke [23]. The Akata Formation is principally composed of marine shale with sandy and silty beds laid down in turbidities and continental slope channel fills, about 7000 m in thickness, serves as the source rock [22]. The Upper Agbada Formation is an array of sandstone and shale deposits [24]. It rests mainly on sand in the upper part alongside limited amount of shale, and contains shale predominantly in the lower part. Over 3,700 m thick, Benin`s upper layers are

enclosed in divers' places with thin layers of laterite of varying thickness, still, are also uncovered bordering the coast. The Somebreiro-Warri Deltaic sand is Quaternary to Recent in maturity and precisely underlies the study area. The dominant aquifer entity in the area falls inside the sands of the upper deltaic top lithofacies [25]. The water table in the study area (the first occurrence of groundwater) is estimated to lie between 4 m to 5 m beneath [26].

In general, sedimentary rocks are taken into consideration to be good aquifers due to their excessive porosity and permeability which arbitrates the hydrogeological settings of the rocks relative to its texture and mineralogy.
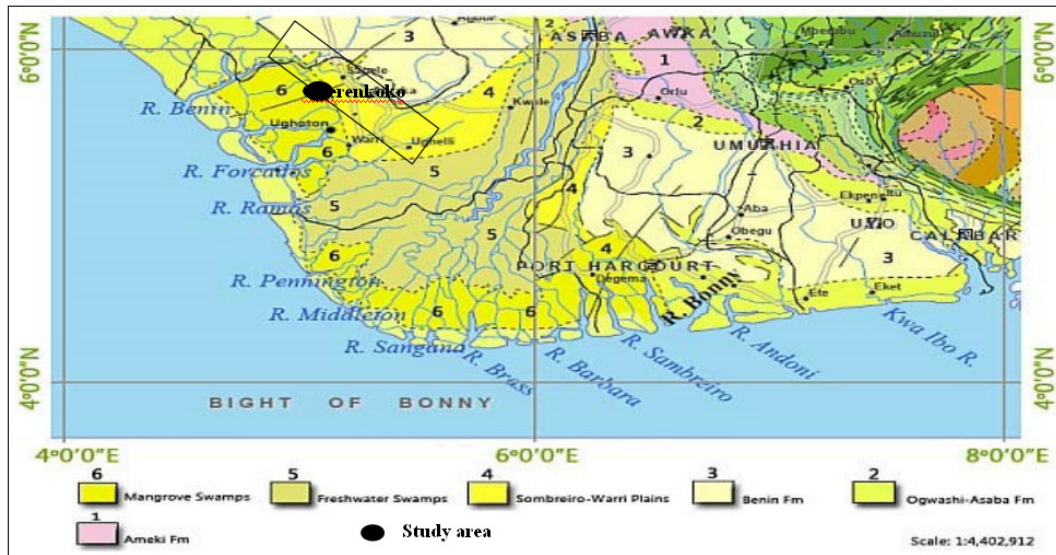

Figure 2. Geological map of the Niger Delta region showing the areal dispersal of mangrove swamps and the Benin Formation.

Source: Adapted from Nigeria Geological Survey Agency, NGSA [18].

3. Methodology

The research methods employed in carrying out this study are geophysical field measurement involving 2-D and 1-D geoelectrical resistivity surveys and geotechnical-soil analysis.

3.1 2-D electrical resistivity tomography (ERT) and 1-D vertical electrical sounding (VES)

In this study, 2-D electrical resistivity tomography data all-inclusive of five (5) parallel and five (5) vertical traverses were measured using a PASI-16GL ground resistivity meter, adopting the conventional Wenner technique (Wenner alpha), on a rectangular grid of 100×80 m^2 in the school premises. Thus, a total of ten (10) 2-D resistivity profiles (data density) were acquired in the study site for a reliable subsoil/geotechnical investigation beneath the school premises. In the Y-direction, 2-D profiles, Ly1 to Ly6 were established and in the X-direction, 2-D profiles, Lx1 to Lx5) were also established as shown in the base map in **Figure 3**. Inter-traverse spacing in the -Y and -X directions is 25 m and 20 m, respectively (**Figure 3**). The 2-D Wenner technique was adopted for this study because it has remarkable depth sensitivity, and because the Wenner array excels at resolving vertical variations in subsurface resistivity (horizontal structures) [8]. The electrode spacing used was 5 m in the -Y and -X directions. In the Y-direction (80 m length) with an electrode spacing of 5 m, a total of 16 electrode positions from 0 to 80 m are occupied by each traverse line, and in the X-direction (100 m length) with an electrode spacing of 5 m, a total of 21 electrode positions from 0 to 100 m are occupied by each traverse line. A total of thirteen (13) vertical electrical soundings were radially run at two positions in the grid adopting the regular Schlumberger method, with half-electrode spacing (AB/2)

varying from 1 m to 200 m. The Vertical Electrical Soundings (VES) involved radial sounding at directions 0°(N-S), 60°(NE-SW), 90°(E-W) and 120°(NW-SE) at positions 1 and position 2 respectively. The vertical electrical soundings (VES 1-13) are acquired to provide subsurface 1-D stratigraphic information to aggregate the 2-D imagery and are performed radially to establish the potential direction of groundwater flow and guide future groundwater practice at the site.

3.2 3-D electrical resistivity tomography (ERT)

To establish a good description of the study site and to minimize the errors arising from the assumption of two-dimensional geometry for geological features, a 3-D resistivity interpretation model that gives the maximum detailed results as opined by Loke [27] was simulated adopting the orthogonal set of measured 2-D apparent resistivity data. The present-day survey cost for 3-D resistivity surveys is equivalently higher than 2-D surveys [27]. Therefore, a comparison of an orthogonal set of 2-D traverse lines was used to generate the three-dimensional (3-D) apparent resistivity data used in this study.

3.3 Geophysical data processing and inversion

The VES data were analyzed by manual curve fitting to establish a resistivity model curve, that was further curve fitted to the standard curve and resulting layer parameters were entered into the Win-Resist computer program [28] and inverted to realize the geoelectric parameters (the layer resistivity, depth and thickness) of the site. In addition, vertical electrical soundings were made radially along different azimuthal angles for a given 'AB/2' interval, so we plotted this to create a polar diagram. For isotropic and uniform strata, this polar diagram is expected to be circular. However, the aberration from the circle to the eclipse indicates an anisotropic nature of the subsurface [29,30] and the possible direction of groundwater flow was inferred from the dominant trend in the polar diagram. The 2-D apparent resistivity data were inverted using the 'Earth Imager 2D program' to generate a 2-D resistivity-depth structure.

To perform 3-D inversion, we assembled the entire orthogonal set of 2-D traverses (that is, in the Y and X directions) into an exclusive 3-D dataset that can be viewed by a standard 3D resistivity inversion software [13,31] using the RES2DINV comparison code. The 3-D apparent resistivity dataset was inverted by applying Earth Imager 3D software and RES3DINV software. Using the Earth Imager 3D software, the entire 3-D dataset was inverted as a block to generate an exclusive three-dimensional resistivity image beneath the subsurface. The RES-3DINV software program uses a process established on smoothing constrained least squares inversion technique [9,32,33] to extract horizontal depth slices in the x-y plane and vertical slices in the x-z and y-z planes from the realized 3-D volume.

3.4 Geotechnical-soil evaluation

A geophysical inversion solution generates a model that should fit the local geology, geophysical field data and be interpretable. However, the principal problem with geophysical inversion is the non-uniqueness problem and one way to minimize this ambiguity is the use of additional data to constrain geophysical inversion solutions [34]. In this study, the accuracy of our geophysical ERT survey was insufficient to completely satisfy the geotechnical exploration requirements; therefore, our geophysical survey was constrained by the results of soil samples collected from three (3) holes on the site (Okerenkoko primary school) as shown on the base map (**Figure 3**). The holes were drilled along traverse 1 (Lx1), traverse 2 (Ly1) and at the center of the grid (**Figure 3**) after the time of this field survey and were confined within the first 8.0 m of each of the three traverses. Soils intended to support engineering structures, pavements, or other loads must be evaluated to predict their behavior under applied loads and variable moisture conditions. In subsoil evaluation, the water content of the soil is very critical to grading its engineering properties. The water content at which soil changes from one state to the other is known as the consistency limit, or Atterberg's limit [35]. The Atterberg limits are an important measure of the critical water content of fine-grained soils: Its shrinkage limit, plastic limit and liquid

limit. Depending on the water content, soil can be in one of four states: Solids, semi-solids, plastics, liquids. Each state has different soil consistency and behavior, and therefore different geotechnical properties [35,36].
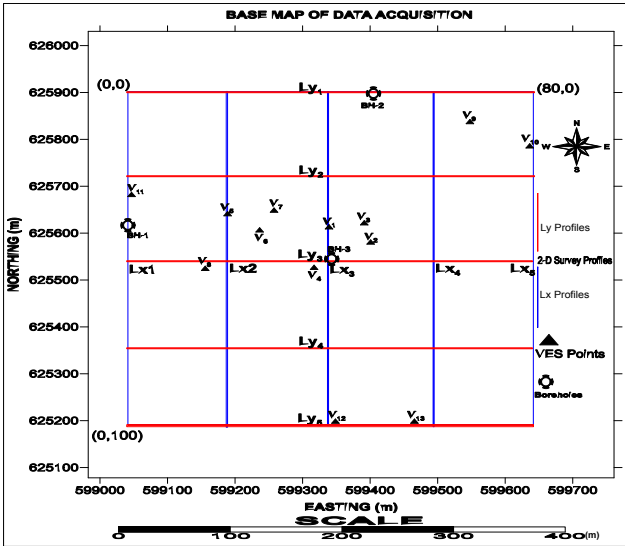
Figure 3. Data acquisition map showing the 2-D resistivity survey grid lines, VES points and Boreholes occupied in the study site (Okerenkoko primary school, Warri-south, Delta State, Nigeria).

The shrinkage limit (SL) is the amount of water above which loss of water does not reduce the sample volume. The plasticity limit (PL) is the amount of water at which a plastic transitions to a semi-solid state, while the liquid limit (LL) is the amount of water at which the soil goes from a plastic state to a liquid state if the soil sample is sufficiently liquid [35,36]. Shrinkage limits are used much less frequently than liquid and plastic limits. The practical importance of the liquid-plastic boundary lies in its ability to reflect the types and amounts of clay minerals present in fine fractions. High values of liquid limit and plasticity index indicate that the soil has high clay and colloidal size of active minerals and that such soil has a poor base for bearing capacity [37].

In this study, soil samples for geotechnical testing were collected in plastic bags and sent to the Soil Research Laboratory at the Department of Earth Sciences, Federal University of Petroleum Resources, Effurun (FUPRE) for analysis. The samples were air-dried and ground into small pieces. The ground sample was then sieved by him through a 4.25 mm aperture. Moisten the sieved soil with a normal concentration of tap water (pH = 7.2), seal the moistened soil in a plastic bag and store for 3 days to meet the British Standard [38].

Fundamental tests performed on soil samples include methods to determine the liquid limit, plastic limit, and plasticity index. These were carried out according to standard practice [38]. The boundary between liquid and plasticity in the soil is called the Atterberg limit.

In each case, the basic requirement is the determination of the water content or moisture content (Wc) of the soil samples at a different number of blows or drops (N).

In each case, the water content (Wc) for each blow was determined using the formula:

$$W_c = \frac{weight\ of\ wet\ soil\ sample}{weight\ of\ dry\ soil\ sample} \times \frac{100}{1} \qquad (1)$$

For soil sample-1 collected from the borehole (BH-1) the number of blows/drops used was 6, 14 and 34 blows and water content was determined for each blow respectively. In soil sample-2 collected from the borehole (BH-2) the number of blows/drops used was 13, 23 and 54 blows and water content was determined for each blow while in soil sample-3 collected at borehole (BH-3) the number of blows/drops used was 18, 23 and 30 blows respectively and water content were determined for each blow.

For liquid limit determination we plotted the water content (Wc) values against the corresponding number of drops, N, on a semilogarithmic graph with water content on the arithmetical/linear scale, and the number of drops on the logarithmic scale. A best-fit straight line was drawn through the plotted points. The water content corresponding to the intersection of the line with 25 (N) drops on the logarithmic axis was read as the liquid limit, LL, of the soil in each sample. The plastic limit was also determined using the procedure and data required for plastic limit determination which involves the determination of the water content in the soil sample after oven drying for a number of trials. The plastic limit was taken as the average moisture content for the number of trails. In each case the plasticity index (I_p) of the soil samples

was determined by finding the difference between the liquid and plastic limits as shown below:

$$I_p = LL\text{-}PL \qquad (2)$$

After determining the liquid limit and plastic limit (Atterberg's limit) of the soil samples, the soil type was classified using the Burmister [39] scheme shown in **Table 1**.

Table 1. Plasticity Indices and Corresponding States of Plasticity (after Burmister [39]).

Soil type	Plastic limit	State of Plastic
1	0	Non-Plastic
2	1-5	Slight
3	5-10	Low
4	10-20	Medium
5	20-40	High
6	>40	Very High

4. Results and discussion

4.1 Vertical electrical sounding (VES)

In a nutshell, the VES model values realized from 1-D resistivity inversion are presented in **Table 2**. The iteration outcome of 1-D inversion for VES 1-6 only shows the sounding curves, inverted layer variables and root mean square (RMS) error depicted in **Figure 4a-4f**. A low RMS error in the order of 6.6%, 2.4%, 2.2%, 2.7%, 3.6%, 2.6%, 3.1%, 2.1%, 2.2%, 2.5%, 2.5%, 2.9%, and 2.8% was actualized in the 1-D inversion of VES 1, 2, 3... to 13 respectively (as shown in **Table 2**). These low RMS errors endorse the accuracy of the VES model resistivity values. Interpretation of VES data brought to light four geoelectric layers within the subsurface classified as topsoil, dry sand, wet sand and peat/clay/sandy clay (**Table 2**). From the layer parameters and inferred lithology shown in **Table 2**, the subsurface is principally sandy in lithology with varying degrees of water saturation. Dry/consolidated sand (ρ between 600 Ωm to ρ ≥ 1000 Ωm) was observed predominantly at the second geoelectric layers from a depth range of 2.9 m to 10.4 m from VES 1 to 13 (**Table 2**). In **Table 2**, it was observed that wet sand (ρ < 200 Ωm), Peat/clay (ρ ≤ 20 Ωm) and Sandy clay (ρ between

20 Ωm to 50 Ωm and below 90 Ωm), were predominant at the third and fourth layers at a depth range of 9.9 m to 27.8 m and beyond 30.0 m respectively. The presence of mechanically weak/unstable Peat/clay/Sandy clay layers at the third and fourth layers at profound depths within the near surface (27.8 m to 30.0 m) apparently shows that the subsurface layers at these depths are weak and not suitable for engineering structures. Although, the dry/consolidated sandy layer observed within the second geoelectric layer is competent as a foundation base for building structures [40], the underlying layers of weak and mechanically unstable peat/clay/sandy clay make it vulnerable to failure. In general, clay soils exhibit unfavorable geotechnical properties (when saturation), due to their low strength, high compressibility and high level of volumetric changes which cause negative defects in engineering structures. This explains the visible cracks/subsidence observed in the buildings at the primary school. The second-layer, third-layer and fourth-layer resistivity maps for VES 1 to 13, are shown in **Figure 5a-5c**. The maps show resistivity variation within the second layers at a depth ranging from 2.90 m to 10.40 m (**Table 2**), third layers at a depth ranging from 9.60 m to 27.80 m (**Table 2**) and fourth layers at a depth beyond 30.0 m. In general, resistivity in sedimentary rocks is influenced by porosity [41], void space, degree of sorting and grain size assessment [42].

For this reason, within each layer, groundwater flows from higher resistivity zones (with low porosity) to lower resistivity zones (with high porosity). This implies that within a layer, areas that are less resistive tend to be more saturated due to high porosity and will have higher water saturation than areas with high resistivity (as indicated in **Figure 5a-5c**). From the second layer resistivity map, it was observed that high water saturation within this layer (depth ranged from 2.9 m to 10.4 m) was predominant in the northeastern and northwestern parts of the site due to low resistivity values (100-700 Ωm) as shown in **Figure 5a**, third layer resistivity map (depth ranged from 9.6 m to 27.8 m) showed high water saturation in the northeastern and western parts of the site, but pre-

dominant in the northeast part with very low resistivity values (40-120 Ωm) as shown in **Figure 5b**. The fourth layer resistivity map showed very high water saturation predominant within this layer (at depth beyond 30 m) as indicated in **Figure 5c**. In **Figure 5a-5c** it was observed that the degree of water saturation in the study site apparently increased with respect to depth, with the fourth geoelectric layer map (**Figure 5c**) showing more zones with a high water saturation than the overlying third and second layers (**Figure 5a-5b**). This observation shows that the subsurface geological structure of the site contains materials with high water content which affects their strength and volumetric properties. These findings reflect the dominance of non-competent materials in the study area. The anisotropy polygon based on the radial VES survey is shown in **Figure 6a-6b**. The dominant resistivity trends (as indicated) show that the flow direction of water is comparable to that depicted in the layer resistivity maps in **Figure 5a-5c**.

4.2 2-D electrical resistivity tomography (ERT)

The outcomes from 2-D ERT for the ten (10) traverses are shown in **Figure 7a-7j**. The 2-D resistivity-depth sections were labeled according to the traverse line directions (**-X** and **-Y**) occupied within the 3-D grid as shown in the data acquisition base map (**Figure 3**). In the (**-X**) direction the 2-D lines were 100 m in length and labeled as (Lx1, Lx2, Lx3, Lx4 and Lx5) while in the (**-Y**) direction the 2-D lines were 80 m in length and labeled as (Ly1, Ly2, Ly3, Ly4 and Ly5). In either case, the subsurface resistivity structure was imaged to reasonable depths suitable for precise assessment of its suitability for engineering practice. Correlating the 2-D resistivity interpretation with resistivity values realized from 1-D inversion (VES survey), it is symbolic of sand lithology with alternating degrees in water content. The 2-D resistivity section for line Lx1 (Traverse 1) with resistivity ranging from 3.7-1113 Ωm is shown in **Figure 7a**. A high resistivity structure (267-1113 Ωm) was observed at depth of 0 to 8.2 m within the subsurface at an electrode position of 0-100 m and indicative of a dry sand layer which was interpreted as the zone of better consolidation favorable

for the construction of building structures. At depths between 8.6 m to 17.1 m, a very low resistivity variation of 3.7-64 Ωm was observed which is symbolic of peat/clay/sandy clay layers, not suitable for engineering practice (**Figure 7a**). The 2-D resistivity section for line Lx2 (Traverse 5) with resistivity ranging from 1.0-10,000 Ωm is shown in **Figure 7b**. A high resistivity structure (1000-10000 Ωm) was observed at depths of 0 to 8.6 m, 1-8.6 m and 0-10.0 m at electrode positions of 5-25 m, 30-60 m and 65-100 m respectively along this traverse. This resistivity value is symbolic of dry sands with little or no water content, which was interpreted as the zone of better consolidation favorable for engineering practice. At depth between 12.8 m to 17.1 m and 6.0 m to 17.1 m at an electrode position of 15-95 m, a very low resistivity variation of 1.0-10 Ωm was observed, which is symbolic to peat/clay layers, not suitable for engineering practice (**Figure 7b**). Between the consolidated layer and peat/clay layer moderate resistivity structure (100 Ωm) was observed sandwiched between these layers and is indicative of wet sand. The 2-D resistivity section for line Lx3 (Traverse 6) with resistivity ranging from 2.9-10,000 Ωm is shown in **Figure 7c**. A high resistivity structure (1302-10000 Ωm) was observed at depth of 0 to 6.0 m at electrode position of 0-100 m along this traverse. This resistivity value is symbolic of dry sands with little or no water content, which was interpreted as the zone of better consolidation favorable for engineering practice. At depths between 4.3 m to 8.6 m and 8.6 m to 17.1 m, moderate (170 Ωm) and very low (2.9-22.1 Ωm) resistivity structures were observed which are symbolic of wet sand and peat/clay layers, respectively (**Figure 7c**). These layers were assessed to be weak and not suitable for engineering practice. The 2-D resistivity section for line Lx4 (Traverse 7) with resistivity ranging from 1.6-7510 Ωm is shown in **Figure 7d**. A high resistivity structure (909-7510 Ωm) was observed at depth of 0 to 8.6 m at electrode positions of 0-85 m and 90-100 m along this traverse. This resistivity value is symbolic of dry sands with little or no water content, which was interpreted as the zone of better consoli-

dation favorable for engineering practice. At depths between 5.0 m to 6.0 m and 6.0 m to 17.1 m, moderate (110 Ωm) and very low (1.6-13.3 Ωm) resistivity structures were observed which are symbolic of wet sand and peat/clay layers, respectively (**Figure 7d**). These layers were also assessed to be weak and not suitable for engineering practice. The 2-D resistivity section for line Lx5 (Traverse 3) with resistivity ranging from 27.8-1758 Ωm is shown in **Figure 7e**. A high resistivity structure (624-1758 Ωm) was observed at depth of 0 to 9.0 m at an electrode position of 0-100 m along this traverse. This resistivity value is symbolic to dry sands with little or no water content, which was interpreted as the zone of better consolidation favorable for engineering practice. At depths between 9.0 m to 13.0 m and 13.0 m to 17.1 m, moderate (221 Ωm) and very low (27.8-78 Ωm) resistivity structures were observed which are symbolic of wet sand and peat/clay/sandy clay layers, respectively (**Figure 7e**). These layers were also assessed to be weak and not suitable for engineering practice. The 2-D resistivity section for line Ly1 (Traverse 2) with resistivity ranging from 38.9-1584 Ωm is shown in **Figure 7f**. A high resistivity structure (627-1584 Ωm) was observed at depth of 0 to 7.0 m at an electrode position of 0-55 m and a depth of 0 to 6.0 m at electrode position of 68-75 m along this traverse. This resistivity value is symbolic to dry sands with little or no water content, which was interpreted as the zone of better consolidation favorable for engineering practice. At depths between 7.1 m to 8.6 m and 8.6 m to 14.3 m, moderate (248 Ωm) and low (38.9-98.0 Ωm) resistivity structures were observed, which is symbolic of wet sand and peat/clay/sandy clay layers, respectively (**Figure 7f**). These layers were assessed to be weak and not suitable for engineering practice. The 2-D resistivity section for line Ly2 (Traverse 8) with resistivity ranging from 21.5-9716 Ωm is shown in **Figure 7g**. A very high resistivity structure (2106-9716 Ωm) was observed at depths of 0 to 5.0 m, 0-4.8 m and 0-7.1 m at electrode positions of 5-15 m, 30-52 m, 55-65 m and 67-75 m respectively along this traverse. This resistivity value is symbolic of dry sands

with little or no water content, which was interpreted as the zone of better consolidation favorable for engineering practice. At depths between 0-7.1 m and 7.1 m to 14.3 m, moderate (457 Ωm) and low (21.5-99.0 Ωm) resistivity structures were observed which is symbolic of wet sand and peat/clay/sandy clay layers, respectively (**Figure 7g**). These layers were also assessed to be weak and not suitable for engineering practice. The 2-D resistivity section for line Ly3 (Traverse 9) with resistivity ranging from 7.9-4871 Ωm is shown in **Figure 7h**. A high resistivity structure (977-4871 Ωm) was observed at depth of 0 to 6.5 m at an electrode position of 5-80 m along this traverse. This resistivity value is indicative of dry sands with little or no water content, which was interpreted as the zone of better consolidation favorable for engineering practice. At depths between 6.5-8.0 m and 8.0 m to 14.3 m, moderate (196 Ωm) and low (7.9-39.3 Ωm) resistivity structures were observed, which is symbolic of wet sand and peat/clay/sandy clay layers, respectively (**Figure 7h**). These layers were also assessed to be weak and not suitable for engineering practice. The 2-D resistivity section for line Ly4 (Traverse 10) with resistivity ranging from 6.1-6442 Ωm is shown in **Figure 7i**. A very high resistivity structure (1130-6442 Ωm) was observed at depth of 0 to 7.1 m of the subsurface at an electrode position of 5-80 m along this traverse. This resistivity value is symbolic of dry sands with little or no water content which was interpreted as the zone of better consolidation favorable for engineering practice. At the near surface (< 5 m) at an electrode position of 0-5 m, a low resistivity structure was observed (**Figure 7i**). At depths between 7.1 m to less than 10 m and 9.0 m to 14.3 m, moderate (198 Ωm) and low (6.1-34.8 Ωm) resistivity structures were observed which are symbolic of wet sand and peat/clay/sandy clay layers, respectively (**Figure 7i**), which are weak and not suitable for engineering practice. The 2-D resistivity section for line Ly5 (Traverse 4) with resistivity ranging from 2.5-9934 Ωm is shown in **Figure 7j**. A high resistivity structure (1249-9934 Ωm) was observed at depth of 0.9 m to 7.1 m at electrode positions of 5-12 m, 0-

6.0 m at electrode positions of 20-25 m, 28-35 m, 37-40 m and 55-75 m respectively along this traverse. This resistivity value is symbolic of dry sands with little or no water content, which was interpreted as the zone of better consolidation favorable for engineering practice. At depths between 7.1 m to 10.7 m and 10.7 m to 14.3 m, moderate (157 Ωm) and low (2.5-19.7 Ωm) resistivity structures were observed which are symbolic of wet sand and peat/clay layers, respectively (**Figure 7j**). These layers were also assessed to be weak and not suitable for engineering practice.

In general, the interpretation of the ten (10) 2-D apparent resistivity-depth sections (**Figure 7a-7j**) showed consistency in their subsurface resistivity structure within the depths imaged in the study area, with a dominance of peat/clay/sandy clay materials

with very low resistivity values observed predominantly at varying depths i.e. 8.6-17.1 m in profile Lx1, 12.8-17.1 m in profile Lx2, 8.6-17.1 m in profile Lx3, 6.0-17.1 m in profile Lx4, 13.0-17.1 m in profile Lx5, 8.6-14.3 m in profile Ly1, 7.1-14.3 m in profile Ly2, 8.0-14.3 m in profile Ly3, 9.0-14.3 m in profile Ly4 and 10.7-14.3 m in profile Ly5 (**Figure 7a-7j**). Therefore, the overlain dry sand layers with high resistivity values at the near surface interpreted as the zone of better consolidation will still suffer from subsidence due to the underlying mechanically unstable peat/clay/sandy clay layers which are highly mobile in response to volumetric changes which cause negative defects to build structures and as a deduction, explains the visible cracks/failure/subsidence observed on structures within the study site (**Figure 1a-1c**).

(a) VES 1 (N-S) Iteration result

(b) VES 2 (E-W) Iteration result

(c) VES 3 (NE-SW) Iteration result

(d) VES 4 (NW-SE) Iteration result

(e) VES 5 (N-S) Iteration result

(f) VES 6 (E-W) Iteration result
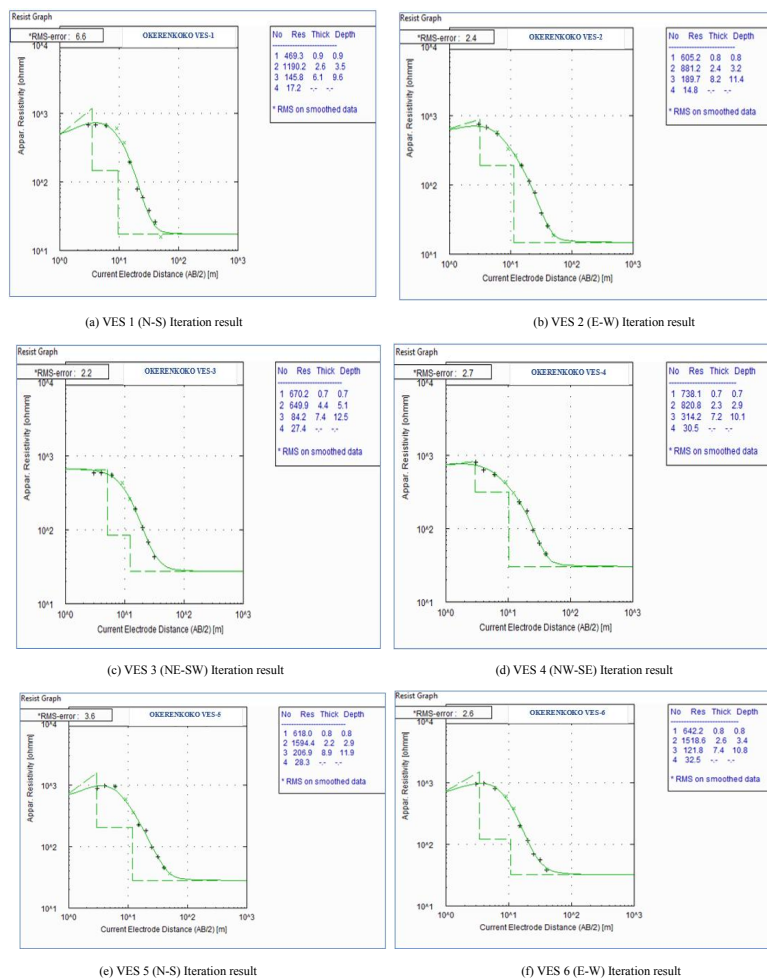
Figure 4(a-f). Iteration results of 1D resistivity inversion for VES 1 to 4 Location 1 and VES 5 and 6 Location 2, showing the resistivity sounding curves and 1-D resistivity models.

Table 2. Summary of VES results in the study site, showing resistivity values, thicknesses, depths and inferred lithology.

VES-No / RMS-Error	Layers		Resistivity (Ω-m)	Thickness (m)	Depth (m)	Inferred lithology
RADAR SOUNDING-1 (VES 1 to 4)						
VES-1 (N-S) RMS: 6.6	1		469.3	0.9	0.9	Topsoil
	2		1190.2	2.6	3.5	Consolidated Sand
	3		145.8*	6.1	9.6	*Wet Sand
	4		17.2	---	---	**Peat/clay
VES-2 (E-W) RMS: 2.4	1		605.2	0.8	0.8	Topsoil
	2		881.2	2.4	3.2	Sand (Dry)
	3		189.7*	8.2	11.4	*Sand (Wet)
	4		14.8	---	---	**Peat/clay
VES-3 (NE-SW) RMS: 2.2	1		670.2	0.7	0.7	Topsoil
	2		649.9	4.4	5.1	Sand (Dry)
	3		84.2	7.4	12.5	**Sandy Clay
	4		27.4	---	---	**Clay
VES-4 (NW-SE) RMS: 2.7	1		738.1	0.7	0.7	Topsoil
	2		820.8	2.3	2.9	Sand (Dry)
	3		314.2*	7.2	10.1	*Sand
	4		30.5	---	---	**Clay/Sandy clay
RADAR SOUNDING-2 (VES 5 to 8)						
VES-5 (N-S) RMS: 3.6	1		618.0	0.8	0.9	Topsoil
	2		1594.4	2.2	2.9	Consolidated Sand
	3		206.9*	8.9	11.9	*Sand
	4		28.3	---	---	**Clay
VES-6 (E-W) RMS: 2.6	1		642.2	0.8	0.8	Topsoil
	2		1518.6	2.6	3.4	Consolidated Sand
	3		121.8*	7.4	10.8	*Sand (Wet)
	4		32.5	---	---	**Clay/Sandy clay
VES-7 (NE-SW) RMS: 3.1	1		790.6	1.0	1.0	Topsoil
	2		1162.1	2.6	3.6	Consolidated Sand
	3		197.3*	6.8	10.4	*Sand (Wet)
	4		38.9	---	---	**Clay/Sandy clay
VES-8 (NW-SE) RMS: 2.1	1		635.6		0.7	Topsoil
	2		1435.4	2.4	3.1	Consolidated Sand
	3		252.8*	7.2	10.3	*Sand
	4		43.5	---	---	**Sandy Clay
VES-9 RMS:2.2	1		443.7	1.1	1.1	Topsoil
	2		1078.3	3.5	4.6	Consolidated Sand
	3		199.6	21.2	25.8	*Sand
	4		17.8	---	---	**Peat/clay
VES-10 RMS: 2.5	1		1150.3	0.7	0.7	Topsoil
	2		961.2	4.8	5.6	Dry Sand
	3		170.9	14.2	19.7	*Wet Sand
	4		24.1	39.7	59.4	**Clay
	5		82.8	--	--	**Sandy clay

Table 2 continued

VES-No / RMS-Error	Layers		Resistivity (Ω-m)	Thickness (m)	Depth (m)	Inferred lithology
VES-11 RMS: 2.5	1		1867.5	1.3	1.3	Topsoil
	2		467.8	9.1	10.4	Sand (Dry)
	3		63.8	61.1	71.5	**Sandy clay
	4		227.3	--	--	Sand
VES-12 RMS: 2.9	1		645.7	0.8	0.8	Topsoil
	2		864.0	3.4	4.2	Dry Sand
	3		148.9	23.6	27.8	*Wet Sand
	4		20.1	--	--	Peat/clay
VES-13 RMS: 2.8	1		266.4	0.8	0.8	Topsoil
	2		760.7	3.2	4.0	Dry Sand
	3		138.5	14.8	18.8	*Wet Sand
	4		16.5	48.6	67.4	**Peat/clay
	5		140.6	--	--	*Wet Sand

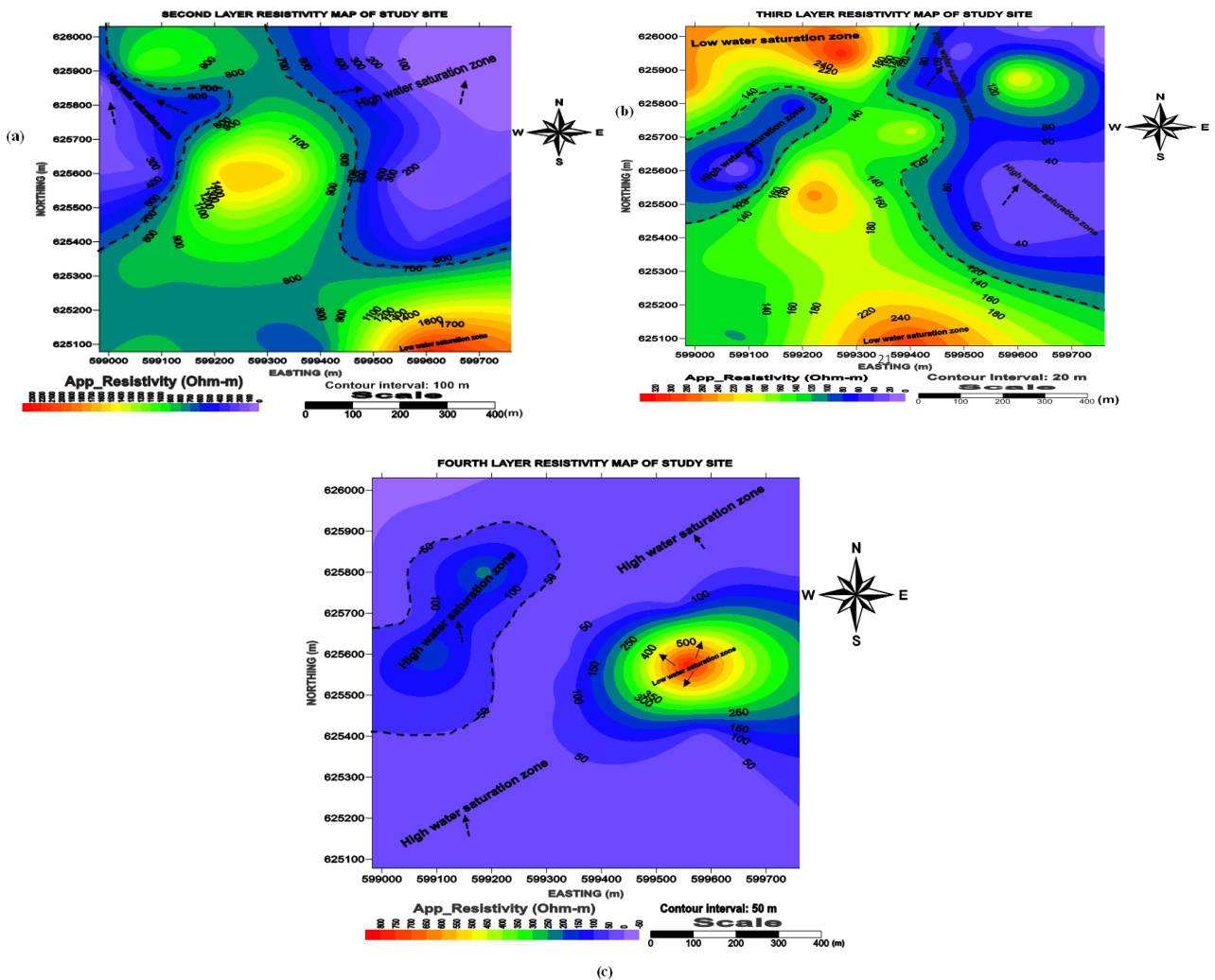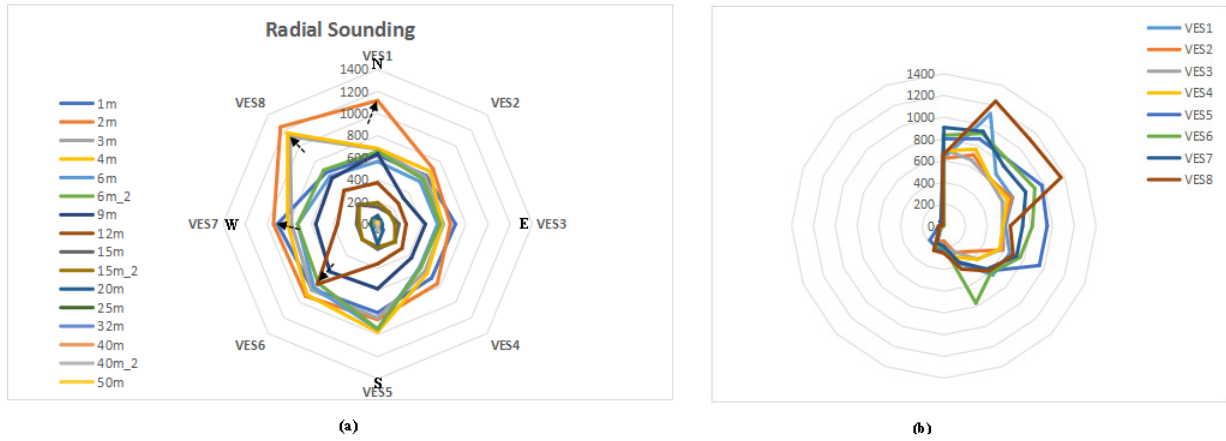*Sandy layer; **Peat/Clay/Sandy clay layer

Figure 5. (a) Second geoelectric layer Map VES 1 to 13; (b) Third geoelectric layer Map VES 1 to 13; (c) Fourth geoelectric layer Map VES 1 to 13. From the maps, resistivity is low towards the northeastern part of the site (see black arrows).
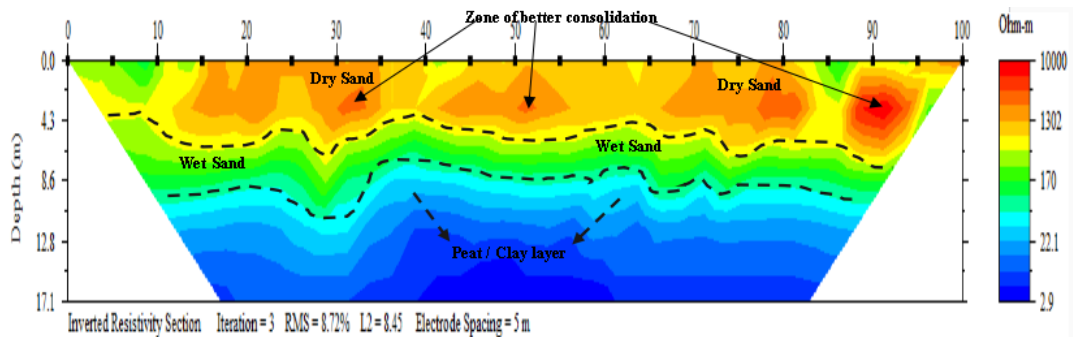
Figure 6. Radar sounding plots (a) polar diagram showing the anisotropy polygon of radar sounding for VES 1 to 8; (b) Chart title for VES 1 to 8 radial sounding.
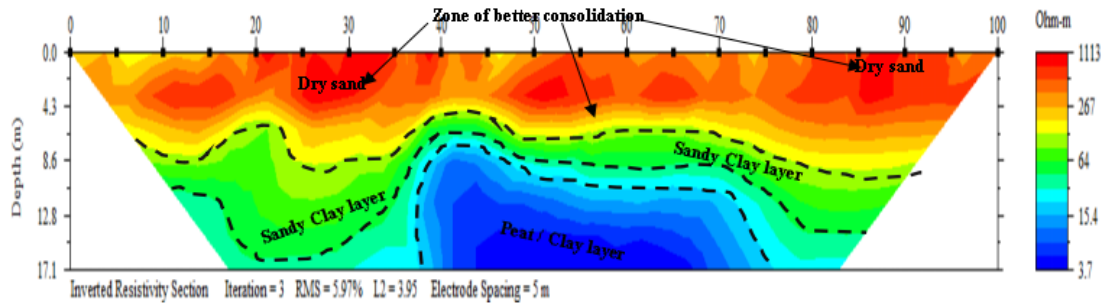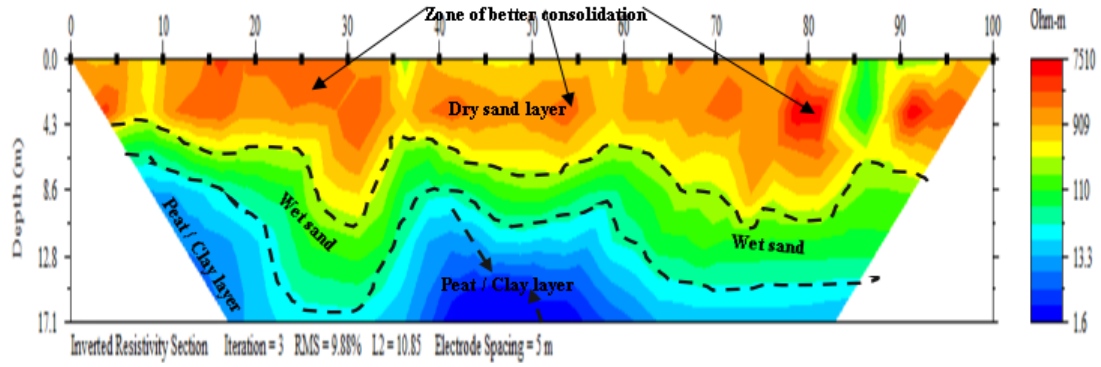

(a) 2D resistivity-depth section for line Lx1 (Traverse 1)
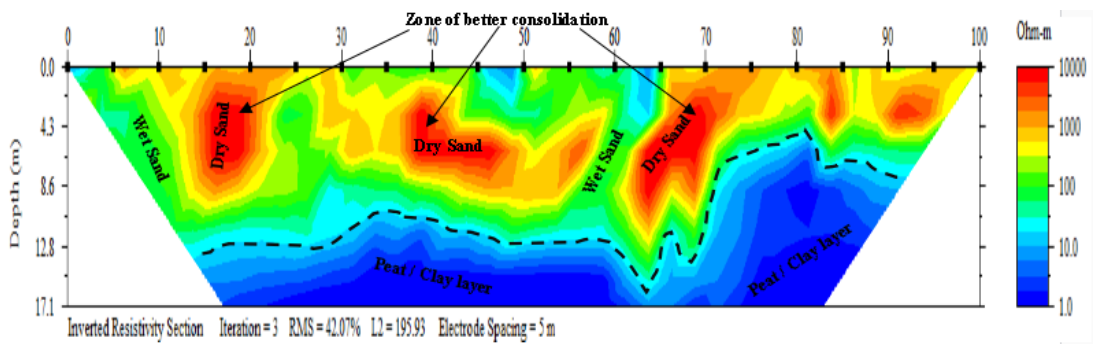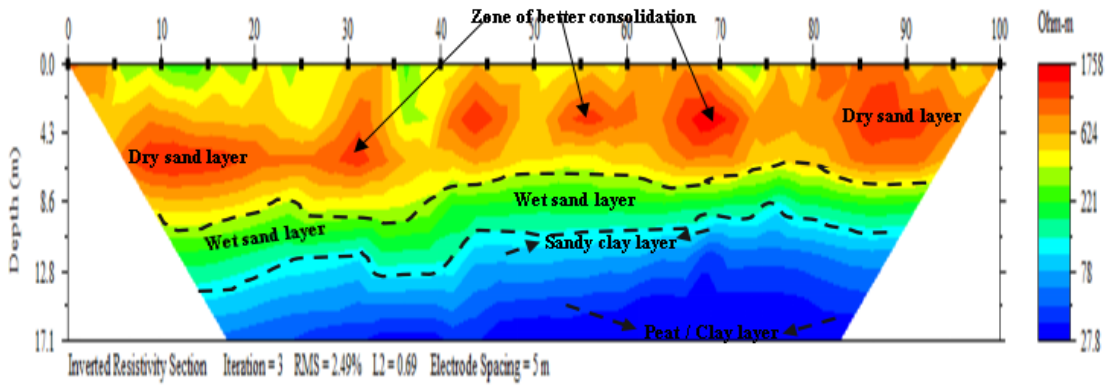

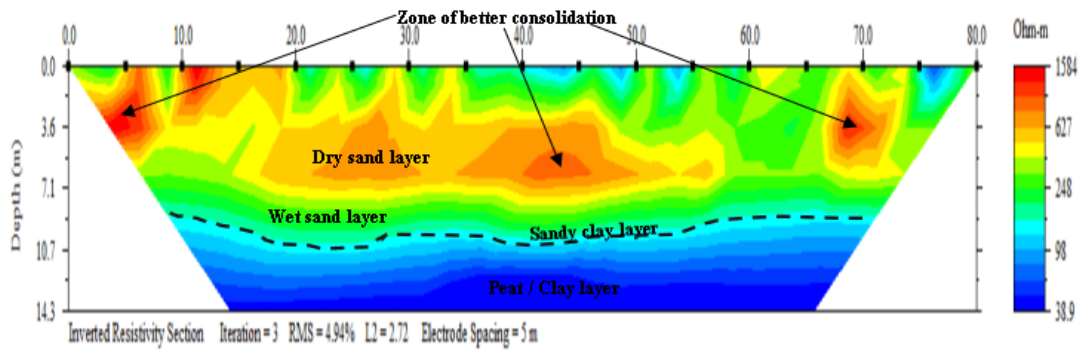(b) 2D resistivity-depth section for line Lx2 (Traverse 5)

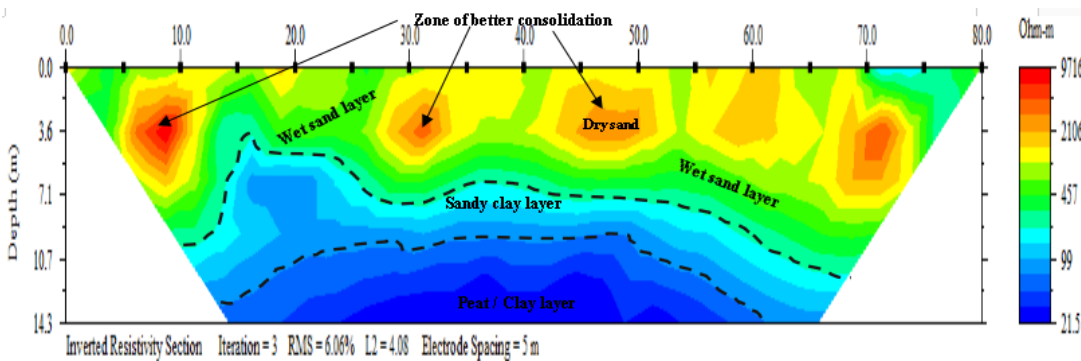(c) 2D resistivity-depth section for line Lx3 (Traverse 6)

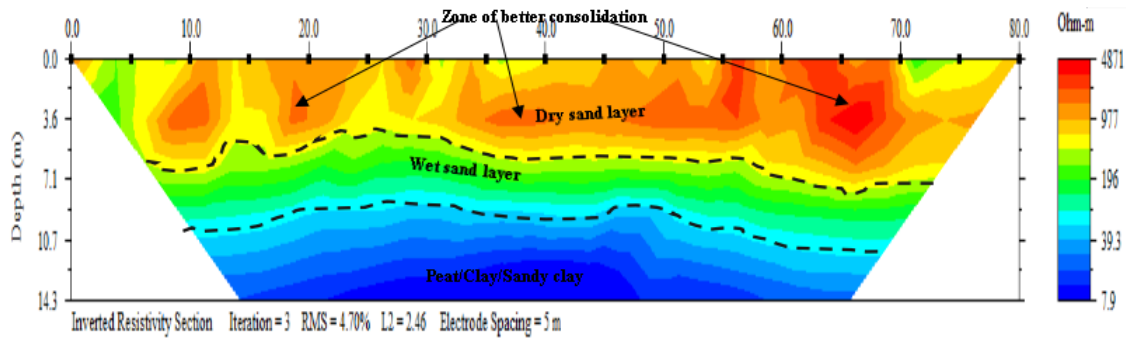(d) 2D resistivity-depth section for line Lx4 (Traverse 7)

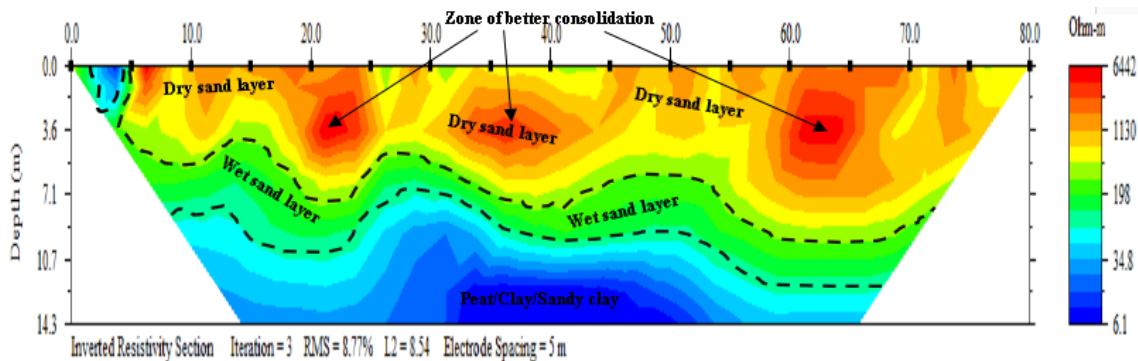(e) 2D resistivity-depth section for line Lx5 (Traverse 3)

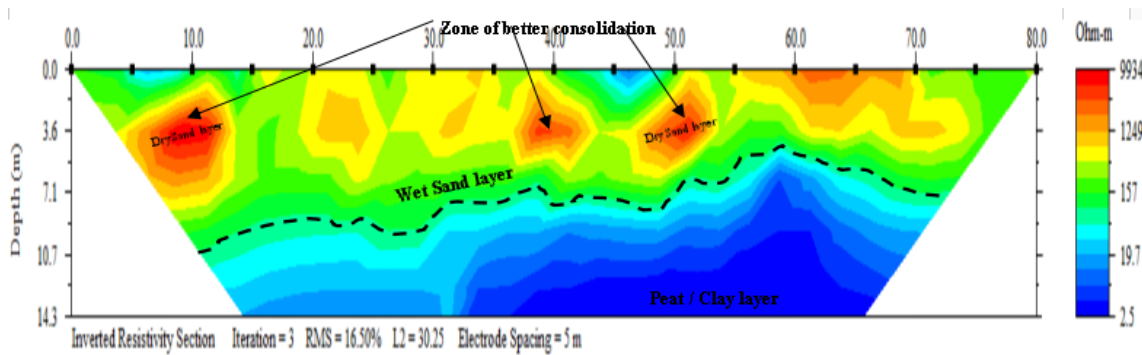(f) 2D resistivity-depth section for line Ly1 (Traverse 2)

(g) 2D resistivity-depth section for line Ly2 (Traverse 8)

(h) 2D resistivity-depth section for line Ly3 (Traverse 9)

(i) 2D resistivity-depth section for line Ly4 (Traverse 10)

(j) 2D resistivity-depth section for line Ly5 (Traverse 4)

Figure 7(a-j). showing the 2D resistivity-depth structure of the subsurface.

4.3 3-D electrical resistivity tomography (ERT)

The 3-D resistivity volume of the study site simulated from the orthogonal set of 2-D apparent resistivity field data is shown in **Figure 8**. The 3-D resistivity volume displays resistivity changes in the vertical, lateral and perpendicular directions down to a depth of 19.8 m within the subsurface. The 3-D volume reflects the dominance of low resistivity materials (11-69 Ωm) which are symbolic of peat/clay/sandy clay layers (as indicated in **Figure 8**). High

resistivity values (2572-15744 Ωm) were also detected at the top, indicative of dry sand. These findings were also observed from the 2-D ERT interpretation shown in **Figure 7a-7j**. Therefore, the low resistivity layers of peat/clay/sandy clay delineated from a depth of 6.6 m to 19.8 m (**Figure 8**) are responsible for the structural failures i.e. cracks/dilapidated structures observed in the buildings (**Figure 1a-1c**) due to mechanical instability and high volumetric changes associated with peat/clay layers, which results in differential settlement over time. This ex-

plains the degree of cracks/damage observed in the school buildings which ranges from moderate to severe risk according to Boscarding and Cording's [17] damage classification.

The 3-D resistivity inversion was also extended by displaying horizontal depth slices and vertical slices from the realized 3-D model volume shown in **Figure 8**. This procedure was actualized using smoothness constrained least-squares inversion process in the RES3DINV program.
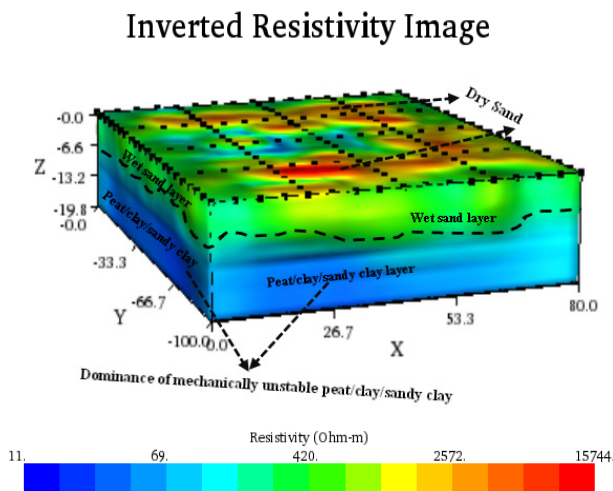
Figure 8. 3-D resistivity tomography volume beneath the study area.

The horizontal-depth slices displayed six layers at depth of 0.00 to 2.50 m in layer 1, 2.50 m to 5.38 m in layer 2, 5.38 m to 8.68 m in layer 3, 8.68 m to 12.5 m in layer 4, 12.5 m to 16.9 m in layer 5 and 16.9 m to 21.9 m in layer 6 (**Figure 9a**). The trend of resistivity variations noted in the 3-D inversion depth slices showed low resistivity materials becoming more evident from the third to the sixth layer. In the first and second layers at depths ranging from 0.00 to 2.50 m and 2.50 m to 5.38 m respectively, high resistivity structures (ρ between 527-1105 Ωm) symbolic of dry sand were observed (**Figure 9a**). In the third layer at a depth ranging from 5.38 m to 8.68 m, a low resistivity structure (ρ between 57.1-120 Ωm) was observed, which is symbolic of sandy clay/wet sand layers (**Figure 9a**). In the fourth, fifth and sixth layers, at a depth ranging from 8.68 m to 12.50 m, 12.5 m to 16.9 m and 16.9 m to 21.9 m respectively, very low resistivity structures (ρ between

6.2-27.2 Ωm) were observed which are symbolic of peat/clay materials within the subsurface (**Figure 9a**). These findings are consistent with the results of 2-D ERT interpretation where the dominance of peat/clay/sandy clay was delineated and observed within a similar depth as imaged in 3-D tomography. Therefore, the subsurface geological structure of the area consists of high-resistivity materials (dry sand) underlain by very low resistivity and mechanically unstable layers of peat/clay/sandy clay which are not favorable for engineering structures within the depths imaged from 2-D and 3-D resistivity tomography. 2-D vertical slices were also extracted from the 3-D depth slices and displayed in the *x-z* and *y-z* plane cells (**Figure 9b-9c**).
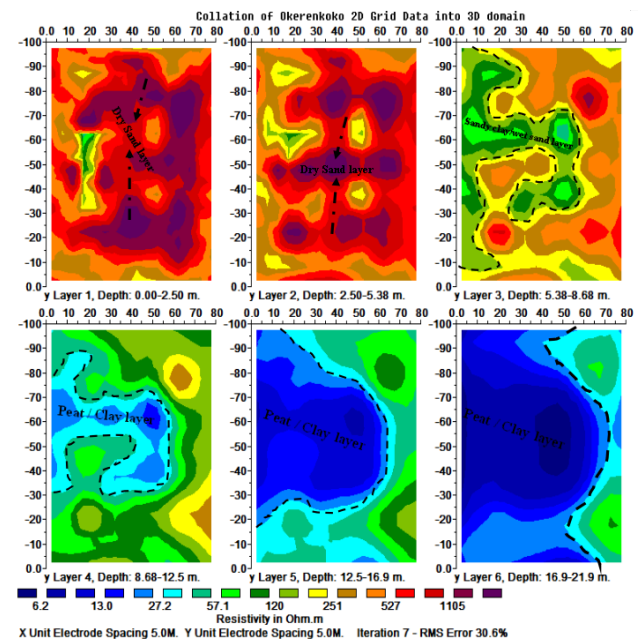
Figure 9a. Six-layer horizontal depth slices obtained from 3-D inversion of orthogonal 2-D profiles using smoothness constrained least-squares inversion.

One of the divergent superiorities of 3-D resistivity inversion over 2-D inversion was checked by matching the 2-D inversion sections in **Figure 7a-7j**, with the 3-D resistivity tomography images and 2-D images extracted from the 3-D inversion models (**Figures 8 and 9**). 3-D resistivity tomography gave continuous variations in apparent resistivity values in all three directions (vertical, lateral and perpendicular) to profound depths of 19.8 m and 21.9 m than in 2-D ERT which imaged the subsurface to a maxi-

mum depth of 17.1 m.

Furthermore, 2-D images extracted from 3-D inversion displayed improved image accuracy and subsurface variation of materials which are based on changes in apparent resistivity values beneath the subsurface in the *x-z* and *y-z* planes within the 3-D grid than in the 2-D inversion sections.

4.4 Geotechnical soil analysis

Geotechnical analysis of soil samples is a necessary requirement for an engineering site characterization program. The water content of the soil samples was evaluated using Equation (1). The results of water content for the three (3) soil samples are presented in **Tables 3-5**.
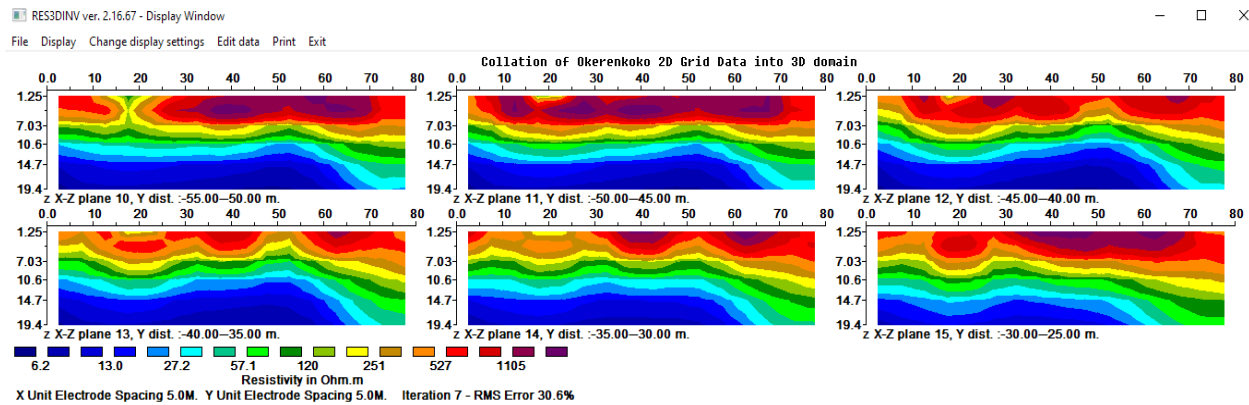
Figure 9b. 2-D vertical slices in the *x-z* plane (10 to 15 plane cells).
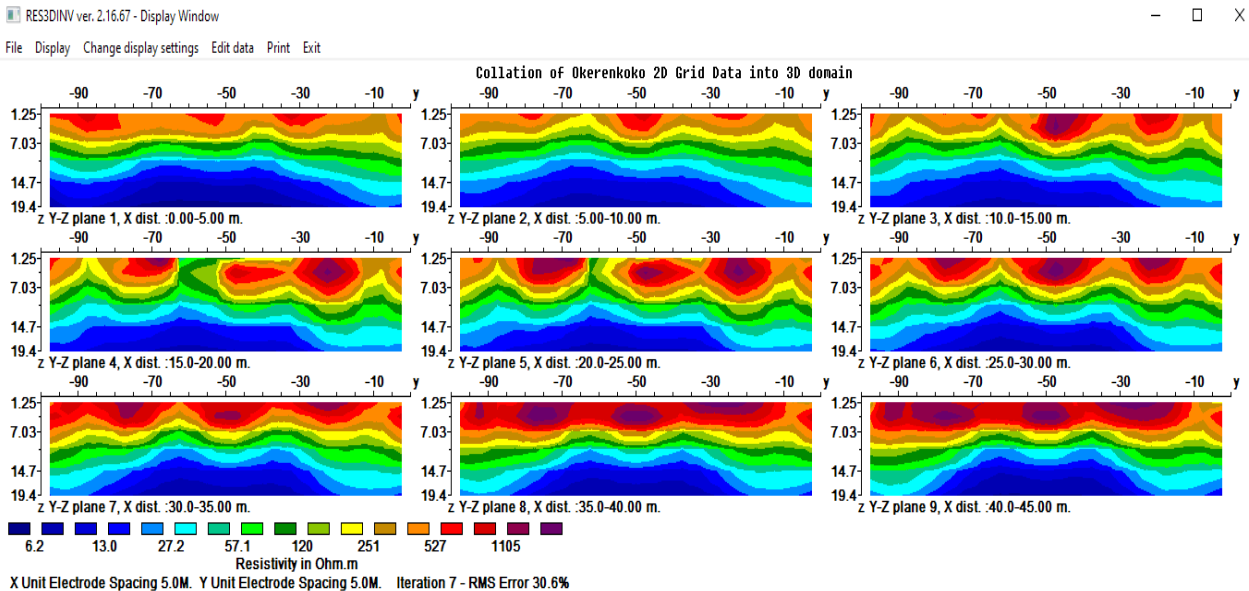

Figure 9c. 2-D vertical slices in the *y-z* plane (1 to 9 plane cells).

Table 3. Summary of number of blows and moisture/water content computed in soil samples-1.

No of Blows	Weight of Wet Sample	Weight of Dry Sample	Water content (%)
6	18.2578	14.8801	22.699
14	21.2831	17.8742	19.072
34	21.7296	19.0331	14.168

From the plot of moisture content against the number of blows for soil sample-1 (**Figure 10**), the moisture content corresponding to 25 blows on the logarithmic axis is the liquid limit, which was read approximately as 13%. Thus, the liquid limit ≈ 13% (**Figure 10**).

The plastic limit was approximated as the average moisture content from **Table 3** which in sample-1 is 18.646.

From the plot of moisture content against the number of blows for soil sample-2 (**Figure 11**), the moisture content corresponding to 25 blows on the logarithmic axis is the liquid limit, which was read approximately 17%. Thus, the liquid limit ≈ 17% (**Figure 11**).

The plastic limit was approximated as the average moisture content from **Table 4** which in sample-2 is 17.130.

From the plot of moisture content against the number of blows for soil sample-3 (**Figure 12**), the moisture content corresponding to 25 blows on the logarithmic axis is the liquid limit, which was read approximately as 13%. Thus, the liquid limit ≈ 13% (**Figure 12**).

The plastic limit was approximated as the average moisture content from **Table 5** which in sample-3 is 13.147.

Figure 10. Plot of moisture content (%) against number of blows for liquid limit determination in soil sample-1.

Table 4. Summary of number of blows and moisture/water content computed in soil samples-2.

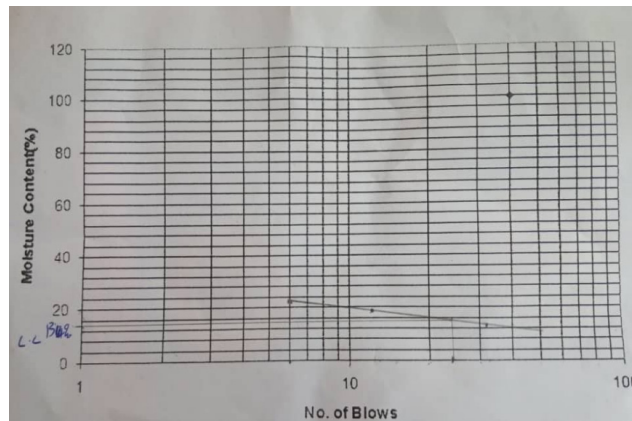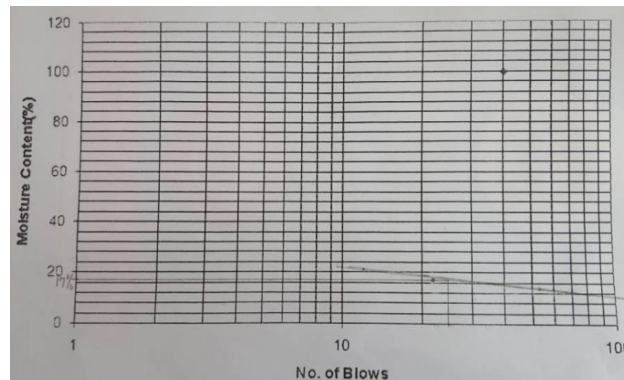| Weight of Container Wo (g)	No of Blows	Weight of Container + Wet Sample W1 (g)	Weight of Wet Sample (g) W1 – W0	Weight of Container + dry Sample W2 (g)	Weight of dry Sample (g) W2 – W0	Moisture content (%)
49.97	13	71.103	21.133	67.57	17.60	20.07
56.184	23	77.136	20.952	74.11	17.926	16.88
67.54	54	89.605	22.065	86.82	19.28	14.45

Figure 11. Plot of moisture content (%) against number of blows for liquid limit determination in soil sample-2.

Table 5. Summary of number of blows and moisture/water content computed in soil samples-3.

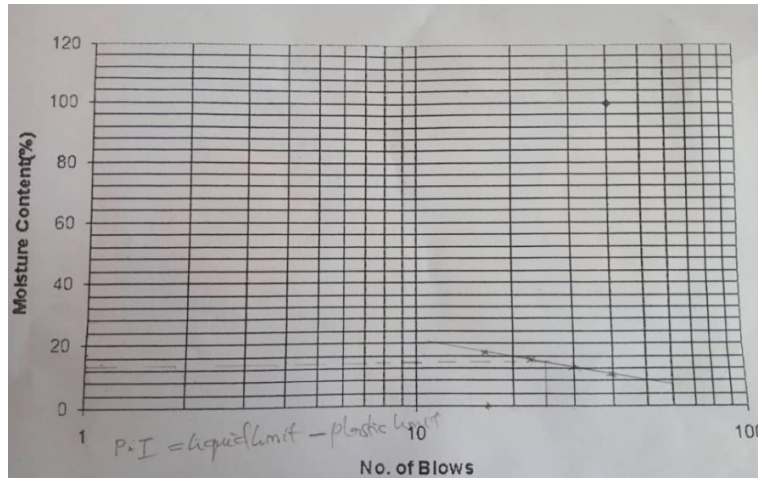| No of Blows	Weight of Wet Sample	Weight of Dry Sample	Water content (%)
18	15.81	13.597	16.2756
23	26.18	23.07	13.4807
30	23.33	21.27	9.6850

Figure 12. Plot of moisture content (%) against number of blows for liquid limit determination in soil sample-3.

The plasticity index (**Ip**) which is the range of water content over which the soil remains in the plastic state, was evaluated for each sample using the relation in Equation (2) recalled as: $I_p=LL-PL$.

For sample-1: Plasticity index (**Ip**) = 13 – 18.646
$$= -5.646 \approx 0 \text{ (zero)}$$

For sample-2: Plasticity index (**Ip**) = 17 – 17.13
$$= -0.130 \approx 0 \text{ (zero)}$$

For sample-3: Plasticity index (**Ip**) = 13 – 13.147
$$= -0.147 \approx 0 \text{ (zero)}$$

The plasticity index parameter (**Ip**) cannot be negative if the plastic limit, in some exceptions is greater than the liquid limit, as observed in soil samples-1, 2, and 3. In this case, it is considered to be zero and the soil is considered non-plastic (**Table 1**), which is symbolic of sandy soil [43,44]. The plasticity of soil is its tendency to undergo deformation without cracking. It is an important index property of fine-grained soil, especially clayey soils. The adsorbed water bounded in clayey soil leads to the plasticity of the soil [44].

In this study, the soil samples were collected within the first 8.0 m of each borehole. At this depth, the soil samples were predominantly composed of sandy soil as delineated from results of 2-D and 3-D

tomography where the subsurface geology from the top-soil to the first 8.0 m consists of sandy soil with varying degrees of saturation i.e. dry sand and wet sand. The clayey soil became more evident from depths beyond 8.0 m in the study area. Therefore, the soil samples analyzed were representatives of sandy soil, and this validates the results of the liquid limit, plastic limit and plasticity index obtained from the soil samples. Sandy soils do not possess any plasticity and their plasticity index is usually assumed to be zero. These findings apparently justify the subsoil conditions defined in the interpretation of the 1-D VES survey and 2-D and 3-D geoelectrical resistivity imaging.

5. Conclusions

2-D and 3-D geoelectrical resistivity imaging supported with geotechnical-soil analysis has been successfully used in evaluating subsoil properties for engineering site investigation at Okerenkoko primary school, in Warri-southwest area of Delta State, to adduce the phenomena responsible for the structural failure observed in the school buildings. The dataset consists of an orthogonal set of ten (10) 2-D geoelec-

trical resistivity lines obtained with the Wenner array and taken as the data density needed for a reliable geophysical-geotechnical exploration study. The dataset was analyzed using the Earth Imager Inversion program and Res3DInv software. The results brought to light the geological structure beneath the subsurface, which consists of four geoelectric layers identified as topsoil, dry/lithified upper sandy layer, wet sand (water-saturated) and peat/clay/sandy clayey soil (highly water-saturated). The profoundly-seated peat/clay materials ($\rho \leq 20$ Ωm) were delineated in the study site to depths of 17.1 m and 19.8 m from 2-D and 3-D tomography respectively. The dominance of mechanically unstable peat/clay/sandy clay layers beneath the subsurface which are highly mobile in response to volumetric changes is responsible for the visible cracks/failure/subsidence observed on structures within the study site. The DC resistivity outcome was validated using the geotechnical study of soil specimens collected from drill holes covering the first 8.0 m on three of the profiles. The consistency limits of the soil samples revealed plasticity indices of zero for all samples. Soil samples within the depth analyzed are therefore representative of sandy soils lacking plasticity and are assumed to have a plasticity index of zero. These findings seem to justify subsurface conditions defined in the interpretation of 2-D and 3-D geoelectric resistivity imaging. In this study, generating a 3D dataset by matching a set of orthogonal or parallel 2D lines improves the speed of field processing, reduces the cost of field logistics and is relevant to obtaining 3D datasets using square or rectangular grid methods. Both 2-D and 3-D resistivity tomography results agreed with each other. 3-D images displayed as horizontal depth slices and the 3-D subsurface volume which were realized in the study, revealed the dominance of very low resistivity materials i.e. peat/clay/sandy clay within the fourth, fifth and sixth layers at depths ranging from 8.68-12.5 m, 12.5-16.9 m and 16.9-21.9 m respectively. Thus, the 3-D inversion model has improved the accuracy level of geoelectrical resistivity imaging, as false elements due to 3-D effects commonly comparable with 2-D inversion images have been reduced in the 3-D inversion images. The research supports near-surface surveys with specific maximum investigation depths of 17.1 m, 19.8 m and 21.9 m for 2-D and 3-D imaging, respectively. The methods employed in this study justifiably provided relevant information on the subsurface geology beneath the study site and its suitability for engineering practice. It is therefore highly recommended to use these methods as important tools for engineering site assessment projects and groundwater inherent investigations.

Conflicts of Interest

We declare that this research work has never been submitted previously by anyone to any journal for peer review and publication; hence it is an original work. All the ethical principles of research in the data collection, preparation, analysis and interpretation were implemented.

Availability of Data and Material

Applicable and available on demand from the corresponding author.

Funding

Acknowledgement

References

[1] Igwe, O., Umbugadu, A.A., 2020. Characterization of structural failures founded on soils in Panyam and some parts of Mangu, Central Ni-

geria. Geoenvironmental Disasters. 7(7), 1-26. DOI: https://doi.org/10.1186/s40677-020-0141-9

[2] Caleb, A.T., Gabriel, I.O., 2012. Geopysical and geotechnical investigation of cham failed dam project, in Nigeria. Research Journal of Recent Sciences. 1(2), 1-18.

[3] Premium Times newspaper Journalism Report in Nigeria, 2021 [Internet]. Available from: https://www.premiumtimesng.com/news/505583-ikoyi-building-collapse

[4] Chendo, I.G., Obi, N.I., 2015. Building collapse in Nigeria: The causes, effects, consequences and remedies. International Journal of Civil Engineering, Construction and Estate Management. 3(4), 41-49.

[5] Akintorinwa, O.J., Adesoji, J.I., 2009. Application of geophysical and geotechnical investigations in engineering site evaluation. International Journal of Physical Sciences. 4(8), 443-454.

[6] Ayolabi, E.A., Enoh, I.J.E., Folorunso, A.F., 2013. Engineering site characterisation using 2-D and 3-D electrical resistivity tomography. Earth Science Research. 2(1). DOI: https://doi.org/10.5539/esr.v2n1p133

[7] Ozegin, K.O., Oseghale, A.O., Audu A.L., et al., 2013. An application of the 2-D D.C. Resistivity method in building site investigation—A case study: Southsouth Nigeria. Journal of Environment and Earth Science (JEES). 3(2).

[8] Loke, M., Chambers, J., Rucker, D., et al., 2013. Recent developments in the direct-current geoelectrical imaging method. Journal of Applied Geophysics. 95, 135-156. DOI: https://doi.org/10.1016/j.jappgeo.2013.02.017

[9] Eze, S.U., Abolarin, M.O., Ozegin, K.O., et al., 2021. Numerical modeling of 2-D and 3-D geoelectrical resistivity data for engineering site investigation and groundwater flow direction study in a sedimentary terrain. Modeling Earth Systems and Environment. 8(1). DOI: https://doi.org/10.1007/s40808-021-01325-y

[10] Aizebeokhai, A.P., Olayinka, A.I., Singh, V.S., 2010. Application of 2D and 3D geoelectrical resistivity imaging for engineering site investigation in a crystalline basement terrain, southwestern Nigeria. Environmental Earth Sciences. 61(7), 1481-1492.

[11] Chambers, J.E., Ogilvy, R.D., Kuras, O., et al., 2002. 3D electrical imaging of known targets at a controlled environmental test site. Environmental Geology. 41(6), 690-704. DOI: https://doi.org/10.1007/s00254-001-0452-4

[12] Bentley, L.R., Gharibi, M., 2004. Two- and three-dimensional electrical resistivity imaging at a heterogeneous remediation site. Geophysics. 69(3), 674-680. DOI: https://doi.org/10.1190/1.1759453

[13] Aizebeokhai, A.P., 2010. 2D and 3D geoelectrical resistivity imaging: Theory and field design. Scientific Research & Essays. 5(23), 3592-3605.

[14] Fargier, Y., Lopes, S.P., Fauchard, C., et al., 2014. DC electricaresistivity imaging for embankment dike investigation: A 3d extended normalization approach. Journal of Applied Geophysics. 103, 245-256. DOI: https://doi.org/10.1016/j.jappgeo.2014.02.007

[15] Hung, Y.C., Lin, C.P., Lee, C.T., et al., 2019. 3D and boundary effects on 2D electrical resistivity tomography. Applied Sciences. 9, 2963. DOI: https://doi.org/10.3390/app9152963

[16] Loke, M.H., 2000. Electrical imaging surveys for environmental and engineering studies: A practical guide to 2D and 3D surveys. Technical Reports. 59.

[17] Boscardin, M.D., Cording, E.J., 1989. Building response to excavation-induced settlement. Journal of Geotechnical Engineering, ASCE. 115(1), 1-21.

[18] Nigeria Geological Survey Agency, 2004. "The Geological Map of Nigeria", A Publication of Nigeria Geological Survey Agency, Abuja.

[19] Asseez, O.L., 1989. Review of the stratigraphy,

sedimentation and structure of the Niger Delta. Geology of Nigeria. Rock View (Nigeria) Ltd., Jos: Nigeria. pp. 311-324.

[20] Reyment, R.A., 1965. Aspects of the geology of Nigeria. University of Ibadan Press: Ibadan. pp. 132.

[21] Short, K.C., Stauble, A.J., 1967. Outline of the geology of Niger Delta. AAPG Bulletin. 51, 761-779.

[22] Doust, H., Omatsola, E., 1990. Divergent/passive margin basins. American Association of Petroleum Geologists: Tulsa. pp. 239-248.

[23] Kulke, H., 1995. Regional petroleum geology of the World, Part II, Africa, America, Australia and Antarctica. Gebruder Borntraeger: Berlin. pp. 143-172.

[24] Merki, P.J., 1970. Structural geology of the Cenozoic Niger Delta. University of Ibadan Press: Ibadan. pp. 251-268.

[25] Akuijeze, C.N., Ohaji, S.M.O., 1989. Iron in Borehole water in Bendel State, Nigeria Association of Hydrogeologist. p. 4011. No.2.

[26] Uchegbulam, O., Ayolabi, E.A., 2014. Application of electrical resistivity imaging in investigating groundwater pollution in Sapele area, Nigeria. Journal of Water Resource and Protection. 6, 1369-1379.

[27] Loke, M.H., 2001. Electrical Imaging Surveys for Environmental and Engineering Studies: A practical guide to 2D and 3D surveys. 62 [Internet]. Available from: http://www.geoelectrical.com

[28] Vander Velpen, B.P.A., 2004. WinRESIST Version 1.0. resistivity sounding interpretation software. M.Sc. Research Project, ITC, Limited: Netherland.

[29] Patra, H.P., Nath, S.K., 1999. Schlumberger geoelectric sounding in groundwater (principle, interpretation and application). M/s A.A Balkema, Rotterdam: Netherlands.

[30] Bankole, S.A., Olasehinde, P.I., Ologe, O., et al.,

2014. Geological and electrical resistivity sounding of olokonla area in north-central Nigeria. Nigerian Journal of Technological Development. 11(1).

[31] Loke, M.H., Baker, R.D., 1996. Practical techniques for 3D resistivity surveys and data inversion. Geophysical Prospecting. 44, 499-523.

[32] Sasaki, Y., 1992. Resolution of resistivity tomography inferred from numerical simulation. Geophysical Prospecting. 40, 453-464.

[33] Eze, S.U., Orji, O.M., Onoriode, A.E., et al., 2022. Integrated geoelectrical resistivity method for environmental assessment of landfill leachate pollution and aquifer vulnerability studies. Journal of Geoscience and Environment Protection. 10, 1-26.
DOI: https://doi.org/10.4236/gep.2022.109001

[34] Sudha, K., Israil, M., Mittal, S., et al., 2009. Soil characterization using electrical resistivity tomography and geotechnical investigations. Journal of Applied Geophysics. 67, 74-79.
DOI: https://doi.org/10.1016/j.jappgeo.2008.09.012

[35] Jamal, H., 2020. Atterberg Limits Soil Classification—Liquid Limit, Plastic Limit, Shrinkage [Internet] [cited 2022 Dec 26]. Available from: www.aboutcivil.org

[36] Seed, H.B., Woodward, R.J., Lundgren, R., 1967. Fundamental aspects of the atterberg limits. Journal of Soil Mechanics and Foundations Division. 92(SM4), 63-64.
DOI: https://doi.org/10.1061/JSFEAQ.0000685

[37] Skempton, A.W., 1953. The colloidal activity of clay. Proceedings of the Third International Conference of Soil Mechanics and Foundation Engineering. 1, 57-61.

[38] British Standard (BS) 1377., 1990. Method of testing soil for civil engineering purposes. British Standard Institute: London.

[39] Burmister, S.V., 1997. Advanced soil mechanics (2nd edition). Wiley and Sons: New York.

[40] Nwankwoala, H.O., Amadi, A.N., Ushie, F.A., et al., 2014. Determination of subsurface geo-

technical properties for foundation design and construction in Akenfa Community, Bayelsa State, Nigeria. American Journal of Civil Engineering and Architecture. 2(4), 130-135. DOI: https://doi.org/10.12691/ajcea-2-4-2

[41] Archie, G.E., 1942. The electrical resistivity log as an aid to determining some reservoir characteristics. Transaction of American Institute of Mining, Metallurgical, and Petroleum Engineers. 146(1), 389-409.

[42] Reynolds, J.M., 1997. An introduction to applied and environmental geophysics. John Wiley and Sons Ltd: Chichester. p. 778.

[43] Sowers, N., 1979. Introductory soil mechanics and foundations: Geotechnical engineering (4th Ed). Macmillan: New York.

[44] Das, B.M., 2006. Principles of geotechnical engineering. Thomson Learning College: Stamford.